

04

## Full-wave 2D modeling of helicons propagation and absorption in the spherical tokamak Globus-M2

© M.A. Irzak, S.A. Nechaev

Ioffe Institute,  
194021 St. Petersburg, Russia  
e-mail: irzak@mail.ioffe.ru

Received August 17, 2021

Revised November 24, 2021

Accepted November 26, 2021

Numerical modeling of propagation and absorption of fast waves (helicons) with frequency 200 MHz in 2D inhomogeneous plasma of the spherical tokamak Globus-M2 was carried out with 2D full-wave code. Toroidal effects, poloidal magnetic field and the actual shape of the flux surfaces were taken into account. The full wave electric field and RF power absorption profiles were computed by solving plasma wave equation with electron Landau damping term. The modeling demonstrated a fairly high efficiency of helicons absorption in the bulk plasma within a wide range of experimental parameters. The waves propagate to the inner regions of the plasma column and are mainly absorbed there; less than 20% of RF energy returns back to the plasma periphery.

**Keywords:** high temperature plasma, nuclear fusion, tokamak, high frequency plasma waves, helicons, plasma wave equation, full-wave code.

DOI: 10.21883/JTF.2022.03.52131.239-21

### Introduction

Modeling of propagation and absorption of helicons (fast waves of intermediate range of frequencies, which, as a rule, are several times higher than the ion-cyclotron frequency) in plasma of large tokamaks with high beta value is of great interest and has been actively performed for the last few years [1–5]. Primarily, it is because the generation of additional current is required in order to control the radial profile of plasma current and to keep the stationary operation mode of tokamak-reactors [6]. Generation of high-frequency (HF) current in the plasma by means of fast waves of intermediate range has been studied for a long time, however, in the early experiments on tokamaks with low beta the efficiency of that method appeared to be low [7]. At the same time, such waves are well absorbed in a dense hot plasma of modern tokamaks and can efficiently generate the current [8]. Besides helicons have a number of advantages in comparison with the use of low-hybrid (LH) waves that have, as a rule, higher frequency, but also belong to the intermediate frequency range. First of all, polarization of the electrical field of fast wave (generally perpendicular to the constant magnetic field) contributes to its absorption a hotter plasma, than LH wave, provided that other conditions are equal. As a result, in large tokamak-reactors with high temperature of plasma, the LH wave cannot get deep inside and is absorbed in peripheral regions, meanwhile helicon enters into plasma considerably deeper and is able to generate HF current in the central regions of plasma. Moreover, unlike the LH waves, there is no criterion of accessibility of the central regions of plasma for helicons [9], which limits permissible longitudinal (i.e. along the magnetic field) slowing down of

the wave from below. Flexible control of the HF current profile can be provided by varying the helicon longitudinal slowing-down and/or its frequency, with results in the shift of its maximum along the minor radius of tokamak within a wide range of limits. Finally, the advantages of helicons, as estimated, refer to higher parametric instability excitation thresholds versus the LH waves, which reduces the parasitic HF power release at the periphery. Moreover, since the electrical field of the fast wave has considerably smaller longitudinal component versus the LH wave, it results in decrease of the harmful effect of a high longitudinal acceleration of electrons near to the antenna. The foregoing is especially relevant for large tokamak-reactors with a high temperature of plasma, for which the numerical calculations have already demonstrated the possibility of efficient application of helicons for the current generation. Nevertheless, the study of perspectives of the helicons use in existing small tokamaks with relatively low temperature is also quite relevant, since there is a possibility to promptly perform the experimental verification. This study provides the results of modeling of propagation and absorption of helicons in plasma of the recently commissioned spherical tokamak Globus-M2 [10,11], where such experiment is planned within the next years. It should be noted that such study is especially relevant for spherical tokamaks having a small aspect ratio (the ratio of the major radius of the plasma to its minor radius). It is because they have relatively high density of plasma at low magnetic field, which results in the problems with conventional methods of HF heating and current drive, in particular, the problem with accessibility of the central regions of plasma for LH waves. This study analyzes the efficiency of absorption of helicons in plasma of the Globus-M2 tokamak based on the

calculation of the structure of electrical field of the excited wave and on the energy absorption profiles.

## 1. Model and calculation parameters

Modeling was performed by means of 2D full-wave code [12] in the model of 2D inhomogeneous plasma of the Globus-M2 tokamak with full consideration of toroidal effects, poloidal cross-section shape and magnetic configuration.

The electrical field of the HF wave  $\mathbf{E}$  was determined by solving the plasma wave equation

$$\Delta \mathbf{E} - \text{grad div } \mathbf{E} + \frac{\omega^2}{c^2} \hat{\epsilon} \mathbf{E} = 0 \quad (1)$$

by using the plasma dielectric permittivity tensor in the form

$$\hat{\epsilon} = \begin{pmatrix} \epsilon & ig & 0 \\ -ig & \epsilon & 0 \\ 0 & 0 & \eta \end{pmatrix} \quad (2)$$

with „cold“ components  $\epsilon$  and  $g$ ; the component  $\eta$  included electron Landau damping term:

$$\eta = 1 - \frac{\omega_{pe}^2}{\omega^2} x_{0e}^2 Z'(x_{0e}) \quad \left( x_{0e} = \frac{\omega}{|k_{\parallel}| v_{Te}} \right), \quad (3)$$

where  $\omega_{pe}$  is the plasma frequency,  $Z$  is the uniform plasma dispersion function,  $v_{Te}$  is the thermal velocity of electrons, and  $k_{\parallel}$  is the component of wave vector along the magnetic field of plasma. The definition of  $k_{\parallel}$  will be given below, which becomes possible as a result of representing the solution  $\mathbf{E}$  as the sum over toroidal and poloidal modes. The electrical field of wave corresponding to an individual toroidal mode  $n_{\varphi}$  was represented as a sum of poloidal modes  $m$ , and, due to poloidal inhomogeneity of plasma, poloidal modes  $m$  are coupled to each other, and thus cannot be considered independently of each other:

$$\mathbf{E}(\psi, \theta, \varphi) = e^{in_{\varphi}\varphi} \sum_{m=-M}^{+M} e^{im\theta} \mathbf{E}^{mn_{\varphi}}(\psi). \quad (4)$$

We introduced generalized toroidal system of coordinates [12] linked to magnetic surfaces, in which  $\psi$  is the „flux“ radial coordinate ( $\psi$  is equal to zero on the axis of discharge and to one at the plasma boundary), and  $\theta$  and  $\varphi$  are poloidal and toroidal angles, accordingly. In toroidal direction, the plasma was considered to be homogeneous, this is why individual toroidal modes  $n_{\varphi}$  can be considered independently of each other. It should be noted that spectral representation of the electrical field of the wave as (4) enables, for each point, correct determination of the longitudinal component of the wave vector for each separate spectral mod as

$$k_{\parallel}^{mn_{\varphi}} = \frac{n_{\varphi}}{R} \cos \alpha + \frac{m}{\sqrt{g_{\theta\theta}}} \sin \alpha, \quad (5)$$

where  $\alpha$  is the angle between full magnetic field and toroidal direction,  $R$  is the major radius, and  $g_{\theta\theta}$  is the component of metric tensor of generalized toroidal system of coordinates ( $\sqrt{g_{\theta\theta}}$  plays the role of a generalized minor radius).

The boundary condition was specified on the surface of plasma for tangential components of the electrical field of wave, which unambiguously defined the field within the whole volume of plasma. Poloidal electrical field was excited at the antenna location, and the presence of an ideal conductive metallic wall was assumed elsewhere. Note that with boundary conditions, in order to obtain correct solution, it is required to provide an efficient mechanism of the HF power absorption in the plasma volume and, as far as possible, to exclude inverse flux of HF power from plasma back to the antenna.

Absorption of HF power at the magnetic surface  $\psi$  averaged over poloidal angle  $\theta$  was calculated by the formula obtained in [13]:

$$\frac{dP_{eLD}}{d\psi}(\psi) = \frac{\omega}{4\pi} \int_0^{2\pi} \text{Re} \sum_m \sum_{m'} e^{i(m'-m)\theta} E_{\parallel}^{m*}(\psi) \times \text{Im}[\eta(\psi, \theta, k_{\parallel}^{m'})] E_{\parallel}^{m'}(\psi) \nu(\psi, \theta) d\theta, \quad (6)$$

where  $\nu(\psi, \theta)$  is the Jacobian of metric tensor of the generalized toroidal system of coordinates, and  $E_{\parallel}^m$  is the projection of  $\mathbf{E}^m$  on the direction of the magnetic field (superscript  $n_{\varphi}$  is omitted here).

2D full-wave modeling requires considerable time; it was performed for a set of parameters of plasma of the Globus-M2 tokamak. A „reference“ case was selected, and then the parameters were varied individually relative to the „reference ones“, that are given below:

- major radius of plasma  $R_0 = 36$  cm, minor radius  $a_0 = 24$  cm, deuterium plasma;
- Shafranov shift on the axis 3 cm, plasma elongation 1.8, triangularity 0.4;
- plasma density  $n_e = (n_{e0} - n_{e1})(1 - \psi^2) + n_{e1}$ ;  $n_{e0} = 6 \cdot 10^{13} \text{ cm}^{-3}$ ,  $n_{e1} = 10^{13} \text{ cm}^{-3}$ ;
- electrons temperature  $T_e = T_{e0}(1 - \psi^2)$ ;  $T_{e0} = 2$  keV;
- vacuum toroidal magnetic field in the center of chamber  $B_0 = 8$  kGs;
- plasma current  $I_p = 500$  kA;
- the antenna is located in the equatorial plane of the tokamak at the low-field side; poloidal size of antenna is  $H_{ant} = 22$  cm;
- frequency of excited wave is 200 MHz;
- supplied HF power is 200 kW;
- the toroidal mode number  $n_{\varphi} = 20$  (it corresponds to the toroidal refraction index of the wave  $N_{\varphi} = ck_{\varphi}/\omega \approx 7$  near to the antenna and  $N_{\varphi} \approx N_{\parallel} = ck_{\parallel}/\omega \approx 12$  in the proximity of the discharge axis).

These parameters fall within the range of planned experiment in the Globus-M2 tokamak, however, selection of some of them has to be additionally explained. In particular, the frequency of 200 MHz and the power of 200 kW are

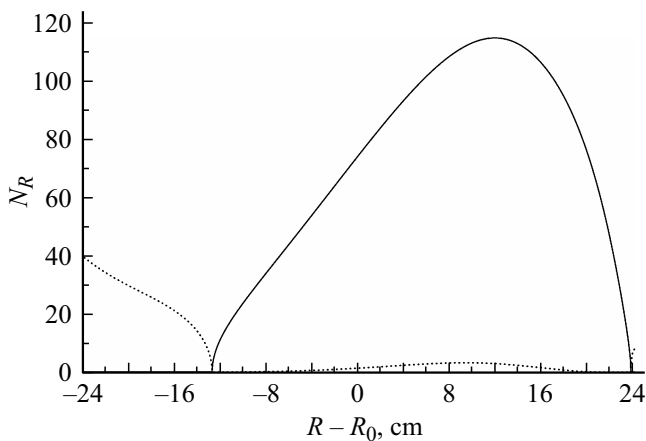


**Figure 1.** Dispersion curves for helicon perpendicular refraction index  $N_R$  along the equatorial plane of the Globus-M2 tokamak for the reference parameters of calculation with zero boundary density. Solid curve refers to real part, dots refer to imaginary part.

conditioned by the available generator. Location of the antenna and its size are determined by the tokamak vacuum chamber port, where it is supposed to locate the antenna. Selection of a high value of the boundary plasma density ( $10^{13} \text{ cm}^{-3}$ ) is related to two important circumstances, which must be explained in detail.

First, in case of the frequency of  $\sim 200$  MHz selected for the helicon excitation, there is always a lower hybrid resonance (LHR) in the area of low densities on the periphery of plasma, and the fast-wave antenna inevitably generates an admixture of a slow wave, whose power will be absorbed near to the LHR. In particular, in case of „reference“ set of parameters of calculation and zero boundary density, the LHR is at the distance of 7 mm from the boundary at the sow-field side. 2D modeling of propagation and absorption of HF wave with the passage through the LHR is possible in practice, however, it requires considerable computational powers due to very small-scale structure of the field of slow wave near to resonance. This is why a quite high density was specified at the plasma boundary ( $10^{13} \text{ cm}^{-3}$ ) — such that there was no LHR within the whole volume of plasma. The issue of LHR impact on the efficiency of a scheme with the use of helicon is important (see, e.g., [5]), but non-trivial, and requires separate study with involvement of other methods.

Second, within the region of low densities at the periphery of plasma, there is a region of non-transparency for helicon located between the boundary of plasma and the surface of the fast wave cut-off. As an illustration, fig. 1 shows dispersion curves for radial component  $N_R$  of the fast wave refraction index at  $n_\phi = 20$  and  $m = 0$ , calculated along the equatorial plane of poloidal cross-section for „reference“ parameters of calculation, but with zero boundary density. A real part of the refraction index  $\text{Re}(N_R)$  is shown as continuous curve, an imaginary part  $\text{Im}(N_R)$  — as dots. It is a result of solution of dispersion equation derived

from (1)–(3) based on the approximation of geometrical optics. By using these data one may obtain geometrical-optical assessment for the single-pass absorption of the wave energy when it propagates through the central region of plasma: it is over 98%, which is quite good. However, the presence of the region of non-transparency at the boundary of plasma results in reflection of a part of HF power back to the antenna. For the parameters in fig. 1 the cut-off on the low-field side is at the distance of 3 mm from the vacuum-plasma boundary, and a portion of the reflected power is about 15%, which is acceptable from the point of view of the efficiency of wave excitation, but it is not good due to the resulting incorrectness of the boundary conditions mentioned above. And in case of higher toroidal refractive indices the width of the region of non-transparency and the height of the barrier are increased, and the problem is aggravating (e.g., for  $n_\phi = 28$  the width of the region of non-transparency rises up to 6 mm, which results in reflection of almost 40% of the supplied power from it). This problem is solved by selection of a high surface density of plasma — the region of helicon propagation begins directly from the boundary. As an example, blue curves (in online version)

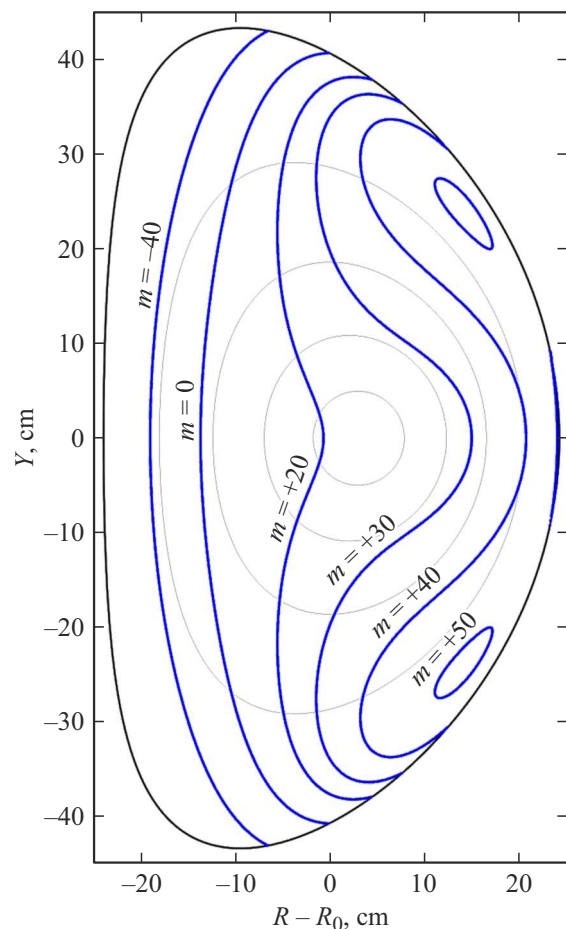


**Figure 2.** Cut-off surfaces for the fast wave in the poloidal cross-section of the Globus-M2 tokamak for toroidal mode  $n_\phi = 20$  and „reference“ parameters of plasma for various numbers of poloidal mode  $m$ .

in fig. 2 show the position of the fast-wave cut-off surfaces in poloidal cross-section of the Globus-M2 tokamak for the „reference“ parameters of plasma (with the boundary density of  $10^{13} \text{ cm}^{-3}$  and  $n_\phi = 20$ ) at different values of the number of poloidal mode  $m$ . The boundary of plasma ( $\psi = 1$ ) is drawn as black line, and thin grey lines refer to magnetic surfaces corresponding to the values  $\psi = 0.2, 0.4, 0.6,$  and  $0.8$ . As we can see on the image, in the majority of cases the main volume of plasma is available for helicon at the low-field side. In particular, for  $m = -40$  only a narrow plasma layer at the high-field side is inaccessible at  $m = 0$  the cut-off is shifted closer to the center, almost to the middle of the minor radius at the high-field side. With further increase of the positive value  $m$  the region of helicon propagation is gradually reducing, so, for the mode  $m = +40$  there is only a narrow region accessible from the low-field side (and at the plasma boundary near to the equatorial plane a narrow region of field of non-transparency appears), and for the mode  $m = +50$  the propagation region virtually disappears. (Note that the values  $|m| \approx 40-50$  are quite realistic and were observed in the calculations described below.)

As it will be seen below from the calculation results, in the majority of cases a quite efficient absorption of

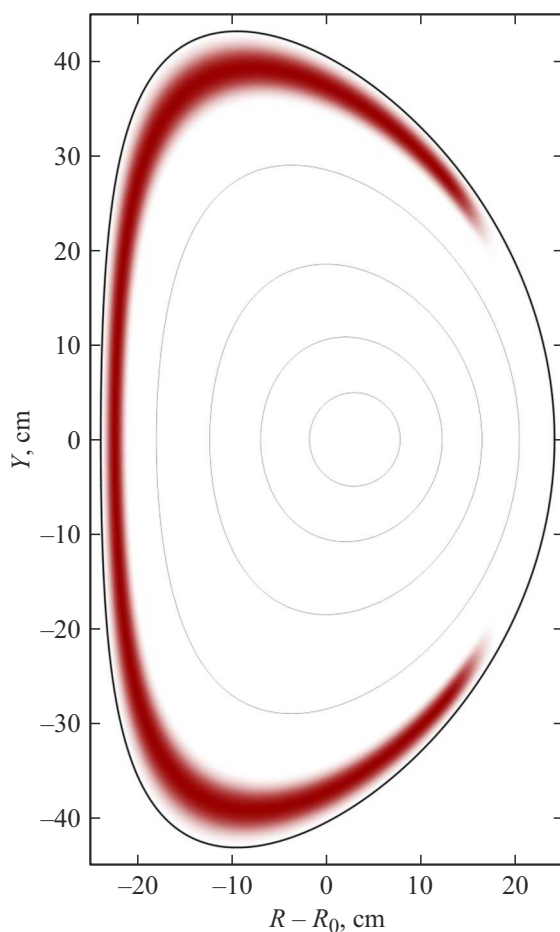


**Figure 3.** Location of artificial peripheral absorbing layer in poloidal cross-section of the tokamak. The darker is the area, the higher is absorption in it.

power in the central regions of plasma is provided, however, a small portion of power returns to the plasma surface, and then is reflected from metallic wall back into plasma. The wave can also be reflected from the cut-off surface, which is located, as a rule, at the high-field side. To assessment of the efficiency of single-pass absorption under the model described above is challenging, because the whole power introduced into plasma will finally be absorbed in the volume of plasma after multiple reflections. In order to assess this effect, an ideal absorbing layer (fig. 3) was placed along the whole surface of plasma at  $\psi = 0.9-1.0$  (except for poloidal region of the antenna location), where the wave incident on it is virtually 100% absorbed and not reflected back. The difference between the total introduced HF power and the fraction of power absorbed in this layer represents the efficiency of „single-pass“ absorption of helicon in the central regions. (The word „single-pass“ is taken in quotes here, because it implies at least double wave passage — first, from the antenna to the central regions of plasma, where absorption may occur, and then back to the plasma boundary.)

## 2. Calculation result

The calculation result for the „reference“ set of parameters is given in Fig. 4:  $a$  is the component of the wave electric field  $\text{Re}(E_1)$ , which is normal to magnetic surface,  $b$  is the component of field  $\text{Re}(E_2)$ , which is tangential to magnetic surface and perpendicular to full magnetic field,  $c$  is the modulus of full field of wave  $|E|$ ,  $d$  is the 2D profile of absorption of HF power (all in arbitrary units). A computational mesh of 361 radial points and 289 poloidal mods was used in order to provide proper accuracy of calculation (the balance between the power introduced into plasma and absorbed power agreed with the error of  $< 1\%$ ).

An explanation to fig. 4,  $d$  is given below. Regarding the spectral decomposition of electrical field in the model of non-uniform plasma, it is unclear how to determine correctly the value of irreversible dissipation of HF power at each point of space, by separating it from the divergence of kinetic power flux associated with the motion of charged plasma particles in the wave field. So, in fig. 4,  $d$  and in the similar figures below we actually show the value of the integrand in the RHS of (6) which is not equal exactly to the local dissipation at a point of space. Keeping this in mind, we nevertheless included these figures in the paper sacrificing the rigorous validation for the sake of illustrative purposes.

The results of modeling are provided below, where some parameters are varied relative to the „reference ones“. The most notable is the dependence on the density and temperature of plasma. In particular, fig. 5 shows distribution of the HF power absorption along the „flux“ (radial) coordinate  $\psi$  at different radial profiles of electron temperature and a

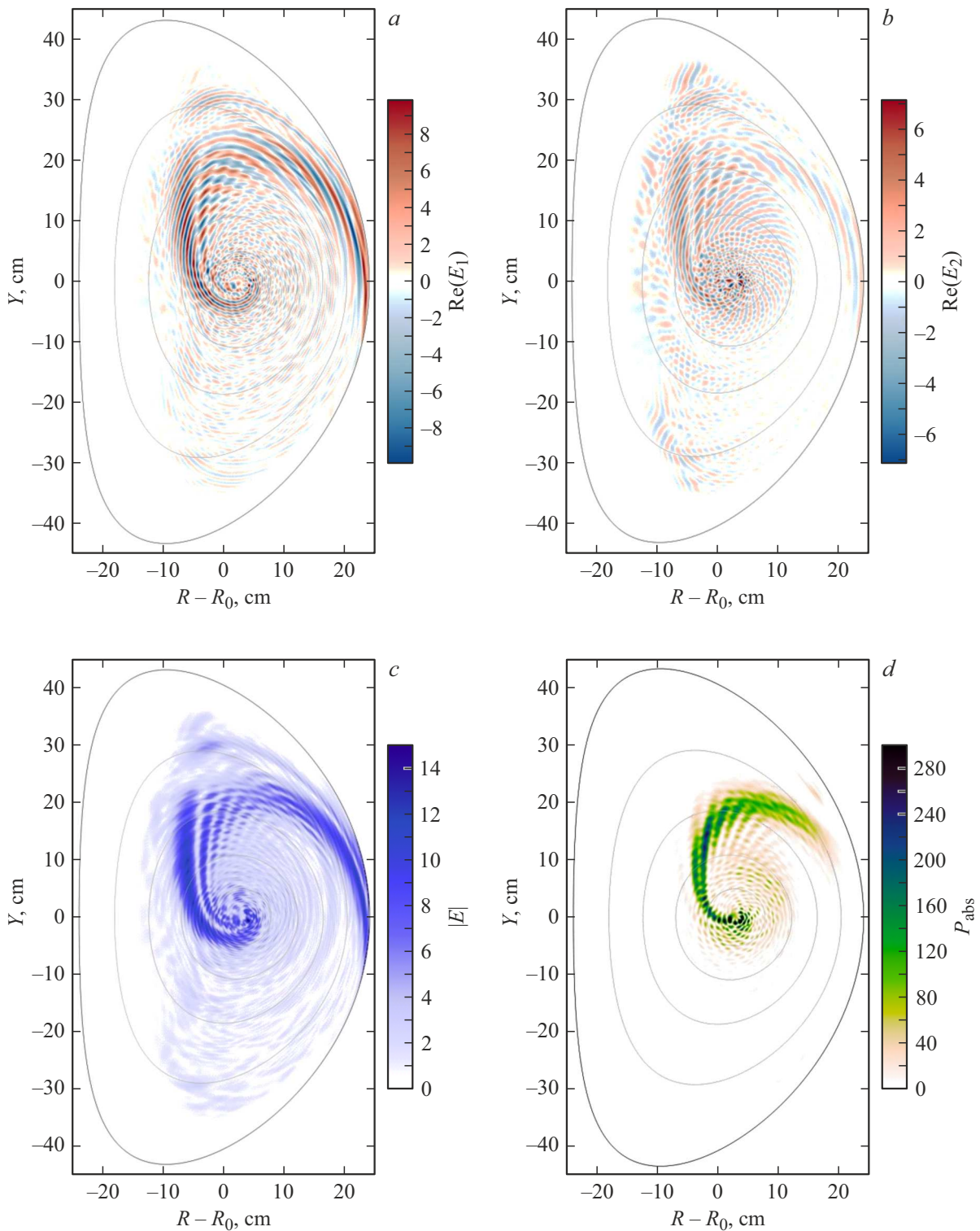


**Figure 4.** The structure of the wave electrical field (*a, b, c*) and absorbed power (*d*) in the plane of poloidal cross-section in case of the „reference“ parameters.

fixed value of the temperature at the axis of discharge  $T_{e0} = 2 \text{ keV}$ . The shapes of profiles are indicated in the figure legend. The value  $dP(kW)/d\psi$  — the HF power absorbed on the magnetic surface corresponding to the radial coordinate  $\psi$  (formula (6)). The area beneath

the curve between two neighboring values  $\psi$  is equal to the power absorbed between two corresponding magnetic surfaces. The area beneath the whole curve is equal to whole HF-power introduced into plasma, i.e. 200 kW. The maximum located on the energy absorption curves

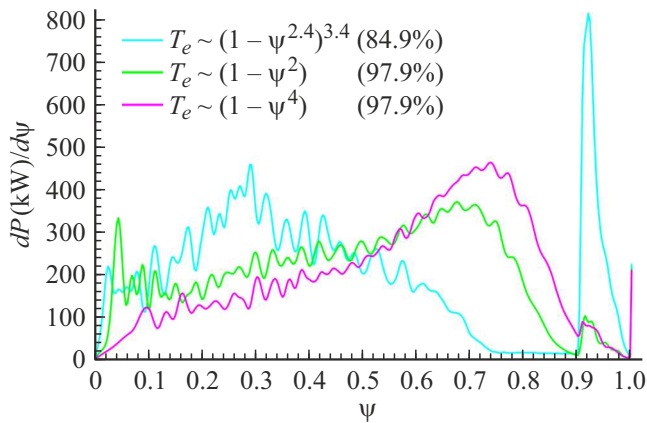


**Figure 5.** Radial profiles of the energy absorption in case of different radial profiles of the temperature.

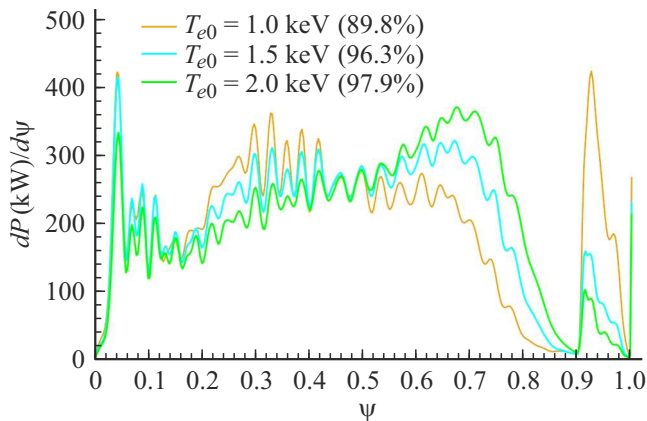


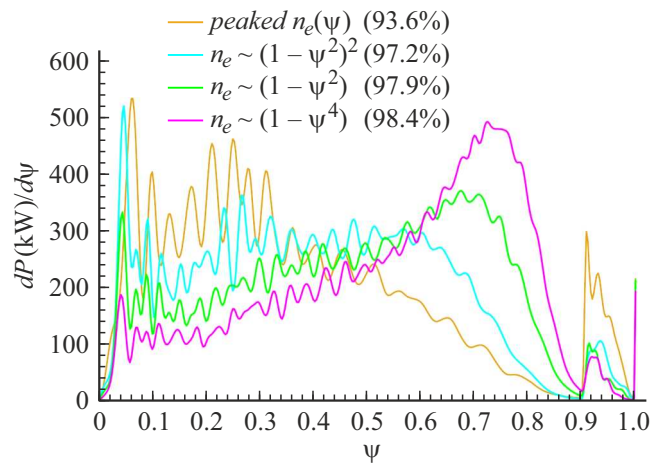
**Figure 6.** Radial profiles of the energy absorption in case of different temperature values in the center.

at  $0.9 \leq \psi \leq 1$  corresponds to the HF power losses in the peripheral absorbing layer; the higher it is, the less efficient is the helicon absorption inside the plasma volume. Efficiency of absorption in the main volume of plasma can be assessed by the portion of HF power absorbed within the range of  $0 \leq \psi \leq 0.9$ ; its value in percent is given in the legend in Fig. 5 for each dependence. Because the efficiency of absorption of HF power is increased as far as the temperature is growing, the obtained results are quite natural. It is seen that in case of parabolic ( $1-\psi^2$ ) and flattened ( $1-\psi^4$ ) profiles of the temperature, main plasma absorbs about 98% of power (green and purple curves (in online version)). At the same time, the temperature profile peaked at the axis ( $1-\psi^{2.4}$ )<sup>3,4</sup> results in decrease of efficiency of absorption in main plasma down to 85% and its considerable growth in peripheral absorbing layer (blue curve (in online version)). In this case, the temperature is high enough only in the centremost regions of plasma for the efficient absorption of HF power by the Landau mechanism. Accordingly, the position of the maximum on the energy absorption profile is also strongly dependent

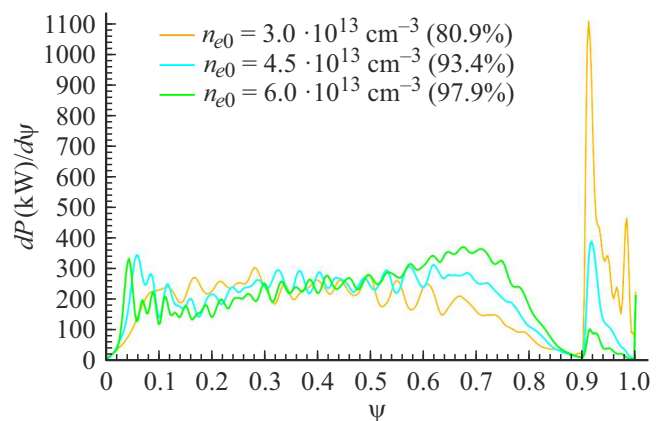
on the temperature profile: for the flattened profile of the temperature, the absorption is shifted to the periphery, and for the peaked profiles — to the center. It should be noted that due to small size of plasma radial profiles of energy absorption appear to be considerably wider than relevant profiles calculated for large tokamaks [1,5].

Fig. 6 shows dependence of the energy absorption profiles on the value of temperature on the discharge axis (for the „reference“ parabolic profile of the temperature). As it should be expected, decrease of the temperature results in the reduction of the energy absorption efficiency (at  $T_{e0} = 1$  keV about 10% of power is lost on the periphery) and shifts the absorption maximum to the center.

Two figures below show similar curves for distribution of absorbed HF power along the minor radius, but in this case depending on the plasma density: on the shape of its radial profile at fixed value on the axis of discharge  $n_{e0} = 6 \cdot 10^{13} \text{ cm}^{-3}$  (fig. 7) and on the value on the axis in case of parabolic profile (fig. 8). Qualitatively, the dependence on the density is of the same nature as that on the temperature, namely: the absorption efficiency



**Figure 7.** Radial profiles of the energy absorption in case of different radial profiles of density.



**Figure 8.** Radial profiles of the energy absorption in case of different density values in the center.

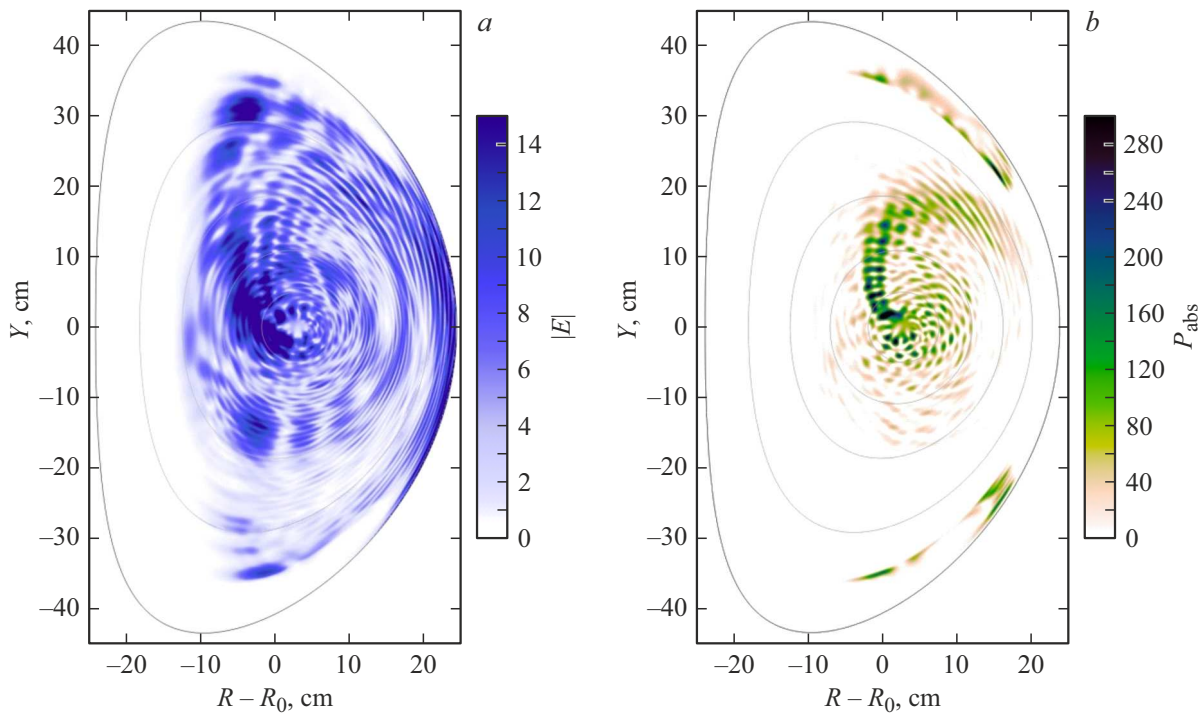


**Figure 9.** The structure of the wave electrical field (a) and absorbed power (b) in the plane of poloidal cross-section with the density at the axis of discharge  $n_{e0} = 3 \cdot 10^{13} \text{ cm}^{-3}$ .

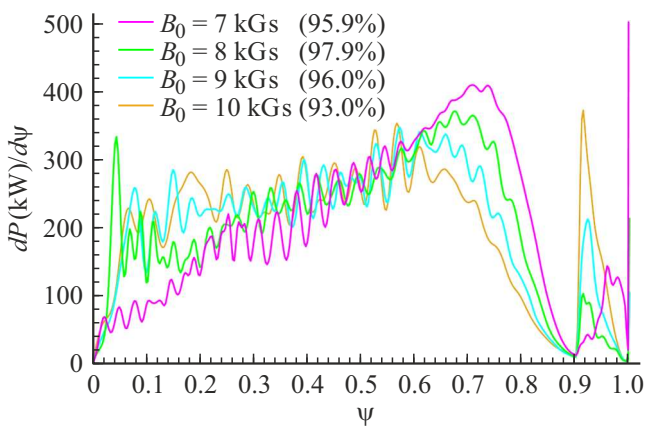


**Figure 10.** Radial profiles of the energy absorption in case of different values of toroidal magnetic field in the center of chamber.

risks with the density increase; peaked density profiles result in more centered absorption and worse efficiency thereof; flattened profiles of density improve efficiency of absorption and shift its region to the periphery. According to fig. 8 it can be seen that a low density of plasma is highly unfavorable for the absorption efficiency: at  $n_{e0} = 3 \cdot 10^{13} \text{ cm}^{-3}$  the highest power losses are observed at the periphery (almost 20%). As a confirmation, fig. 9 shows 2D profiles of full electrical field of the wave (fig. 9, a) and local absorption of the HF power (fig. 9, b). The wave field fills almost whole volume available for it, and a clear

interference pattern is observed. A significant release of power is also seen on the periphery.

Fig. 10 shows radial profiles of energy absorption depending on the value of toroidal magnetic field  $B_0$  in the center of chamber. In general, reduction of the magnetic field is favorable for the efficiency of absorption, however, LHR appears at the boundary of plasma in case of the field of 7 kGs (spike on purple curve (in online version) at  $\psi \approx 1$ ), thus deteriorating the efficiency of helicon excitation and reducing the accuracy of calculations. Fig. 11 shows radial profiles of energy absorption depending on the value of the plasma current  $I_p$ . It is seen that lower currents result

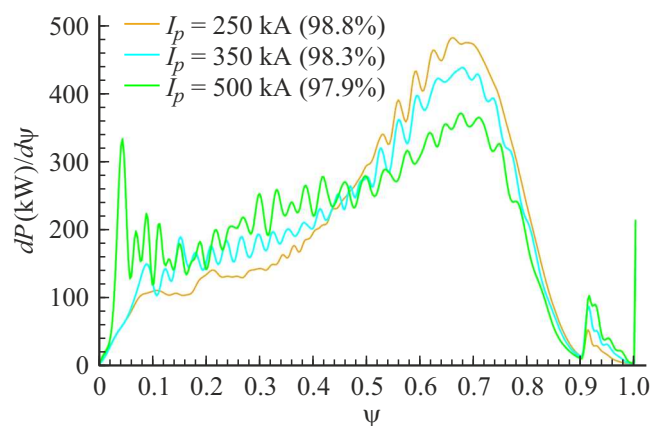


**Figure 11.** Radial profiles of the energy absorption in case of different values of the plasma current.

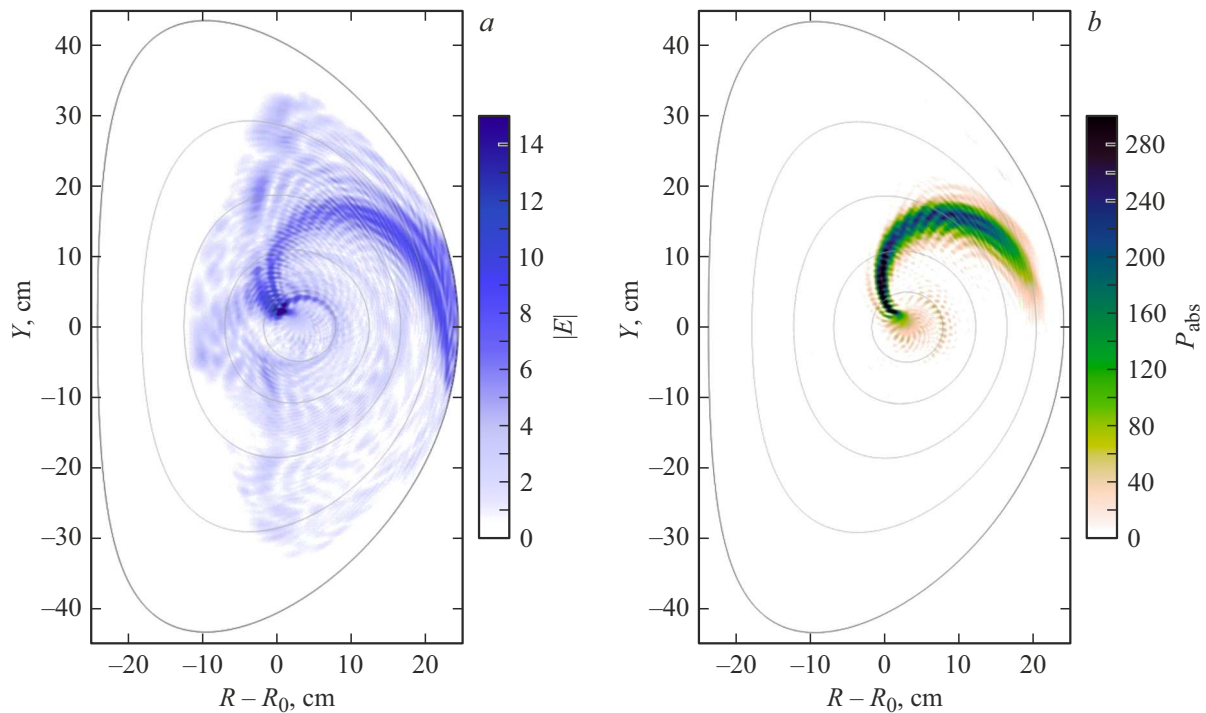


**Figure 12.** Structure of the wave electrical field (a) and absorbed power (b) in the plane of poloidal cross-section at the plasma current of 250 kA.

in a moderate improvement of the absorption efficiency (one should also note that the current reduction, along with the shear change, leads to a considerable reduction of the value of full magnetic field). A beneficial effect of the plasma current reduction can be observed in fig. 12, where 2D profiles of the field of wave and energy absorption are shown for the low plasma current value  $I_p = 250$  kA. The cone of HF power absorption shown in fig. 12, b has a clearly outlined and maximally smooth shape indicating efficient single-pass absorption (compare it with the energy absorption profiles in fig. 4, d and 9, b).

Studying the impact of the sign (i.e. direction) of toroidal magnetic field  $B_0$  and the plasma current  $I_p$ , with other parameters unchanged, appeared to be quite interesting. Until now all presented results were obtained for a positive sign of the magnetic field and the plasma current relative to toroidal direction (i.e. both the field, and the current were directed from the plane of 2D figures towards us). Fig. 13 shows the change of radial profile of energy absorption with the change of signs of magnetic field and plasma current (in all four cases  $n_\phi = +20$ , i.e. the wave was propagating in in positive toroidal direction). It is seen, that the change of sign of the magnetic field with preservation of the direction of current does not impact radial profile of absorption of the HF power, but the change of direction of the plasma current while keeping the direction of the magnetic field results in considerable rearrangement of the energy absorption profile. In fact, the change of the magnetic field direction, of course, also impacts the result — it just cannot be viewed on a one-dimensional graph.

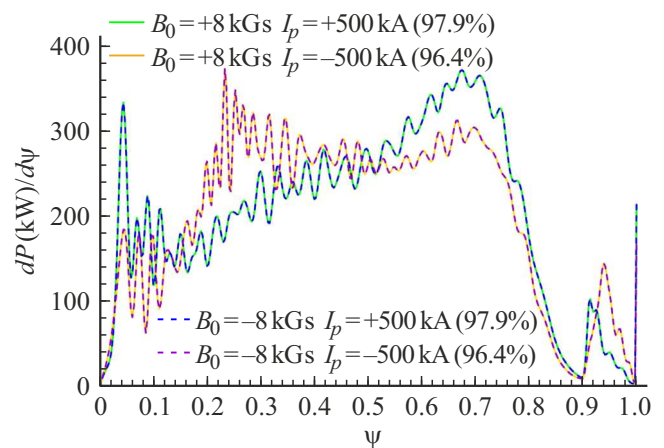


**Figure 13.** Radial profiles of the energy absorption in case of different directions of toroidal magnetic field and the plasma current.

Fig. 14 shows how the change of directions of the vacuum magnetic field and plasma current restructures the 2D profile of energy absorption. In case of the change of the magnetic field sign only, one-dimensional radial profile of absorption is not changed, the two-dimensional structure also remains, but is inverted relative to the equatorial plane (see the pairs (a)↔(c) and (b)↔(d) in fig. 14). It is because a helicon propagates mainly along magnetic line of force going progressively deeper inside the plasma and following a spiral path (for  $n_\phi > 0$  it advances in the positive toroidal

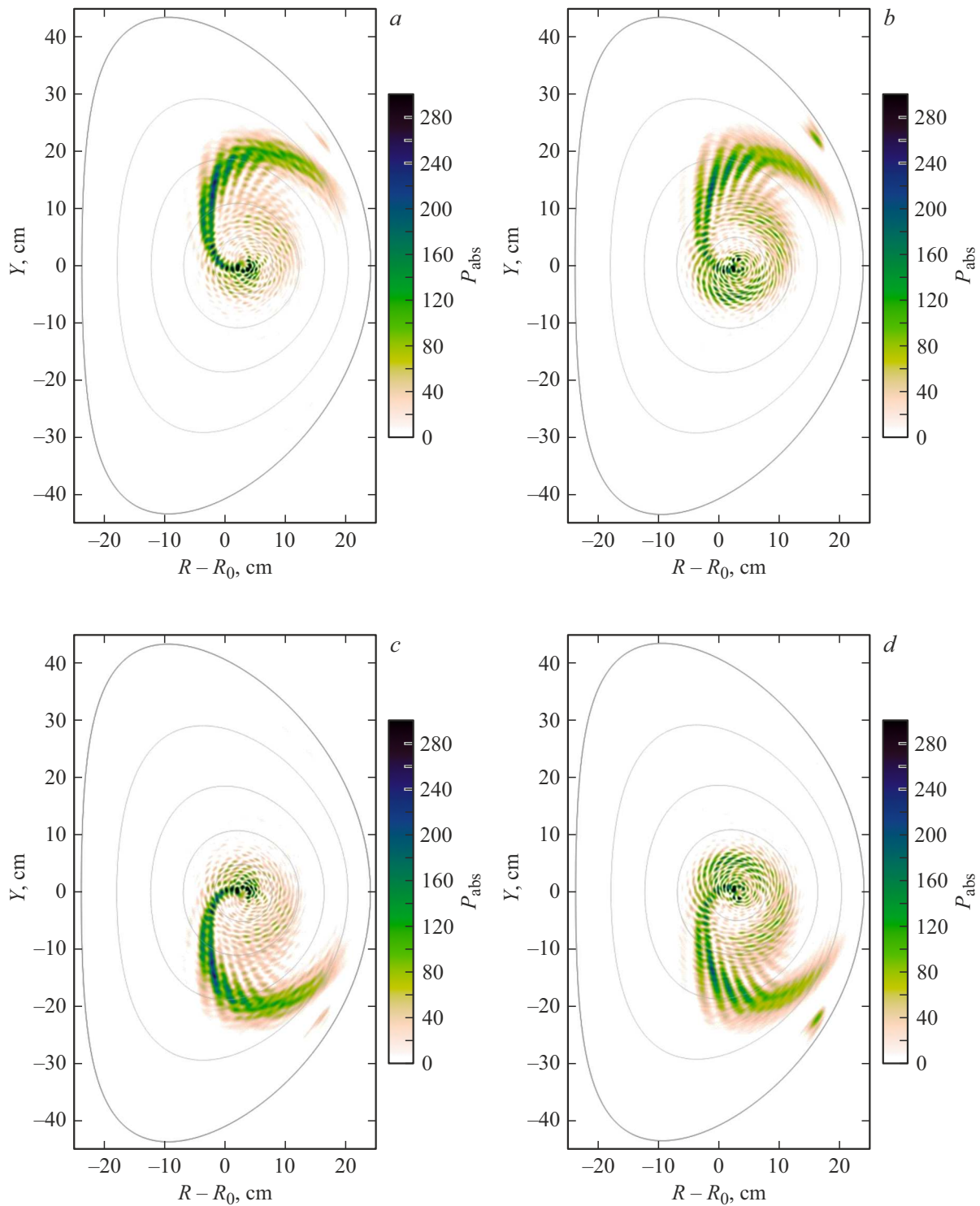


**Figure 14.** The energy absorption profiles in the plane of poloidal cross-section with different directions of toroidal magnetic field and the plasma current: *a* —  $B_0 = +8$  kGs,  $I_p = +500$  kA; *b* —  $B_0 = -8$  kGs,  $I_p = -500$  kA; *c* —  $B_0 = -8$  kGs,  $I_p = +500$  kA; *d* —  $B_0 = +8$  kGs,  $I_p = -500$  kA.

direction, i.e. from the plane of figure to us). If  $B_0$  and  $I_p$  are oriented in the same direction, then, moving in the positive toroidal direction, the line of force at the same time goes upward from the antenna, curling counter-clockwise in the plane of poloidal cross-section, which agrees with

the behavior of the wave in fig. 14, *a, b*. If  $B_0$  and  $I_p$  have different signs, then, moving in the positive toroidal direction, the line of force at the same time goes down from the antenna, curling clockwise in the plane of poloidal cross-section; it is what we see in fig. 14, *c, d*.

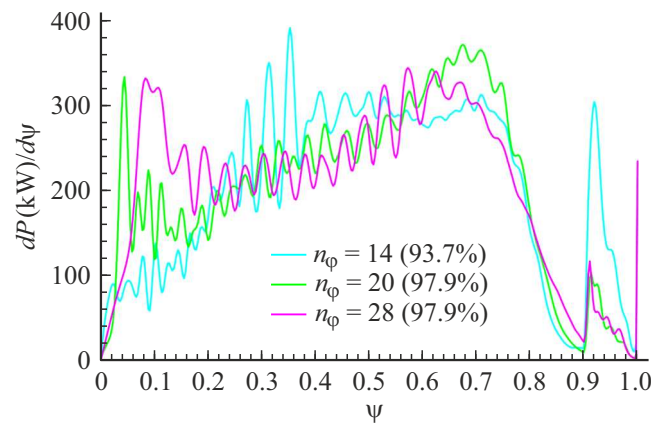


Figure 15. Radial profiles of energy absorption for different numbers of toroidal mode  $n_\phi$ .

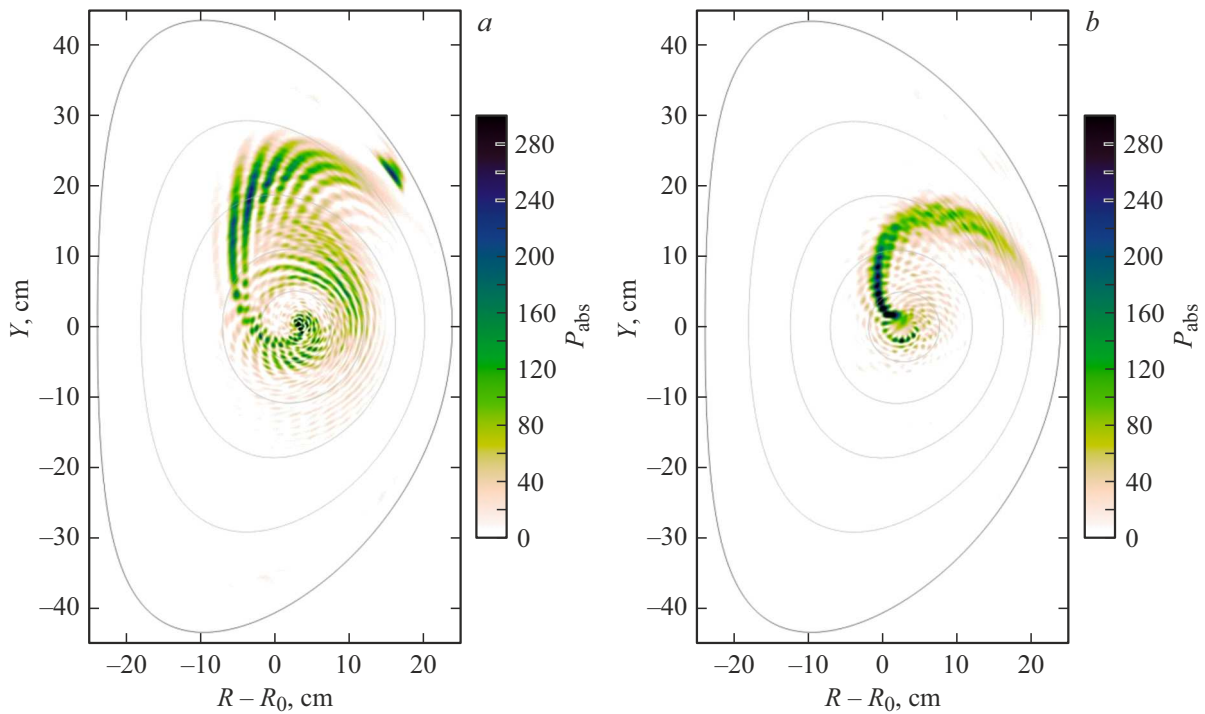


Figure 16. Energy absorption profiles in the plane of poloidal cross-section for  $n_\phi = 14$  (a) and 28 (b).

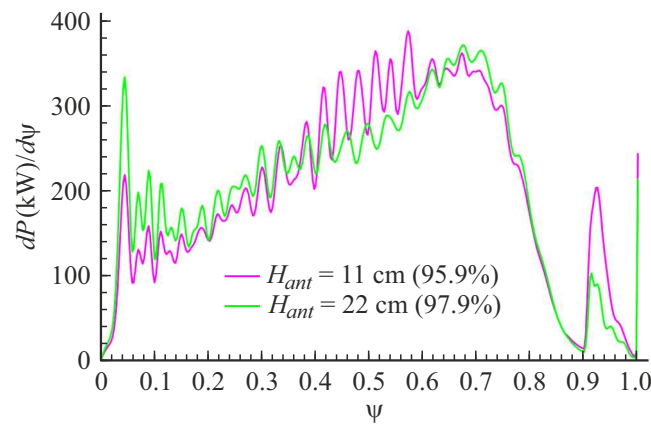
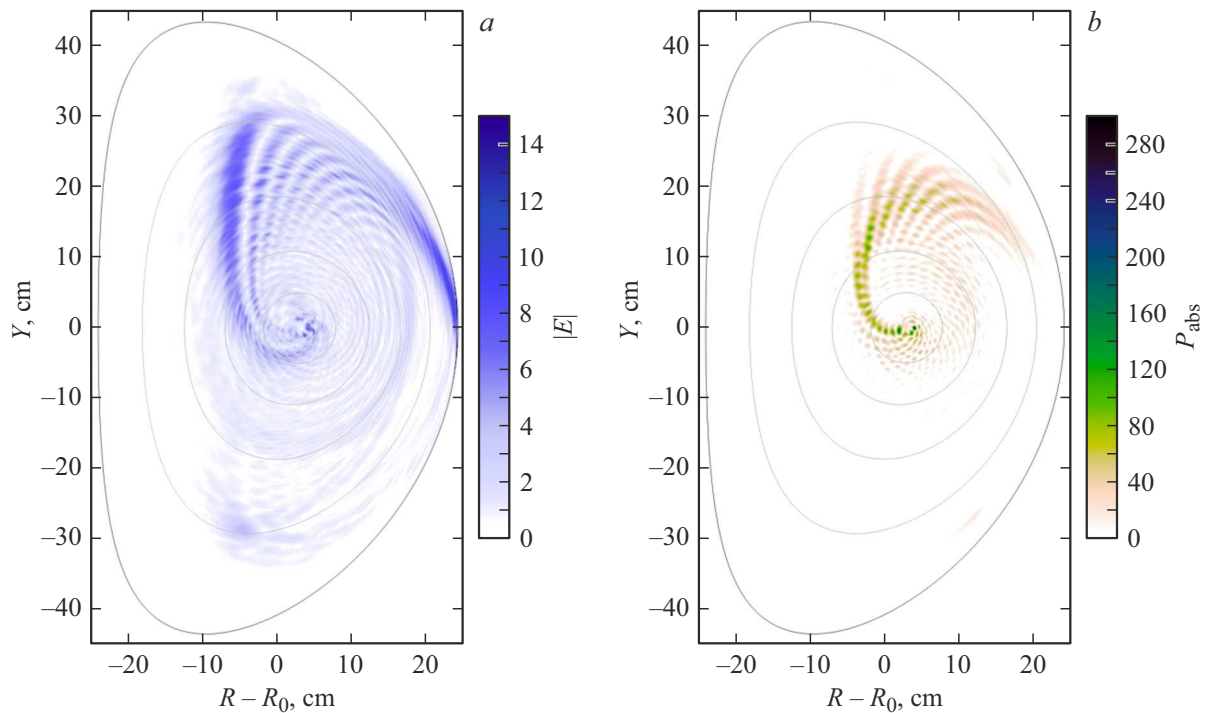


Figure 17. Radial profiles of energy absorption for the antennas of different heights.



**Figure 18.** Structure of the wave electrical field (a) and absorbed power (b) in the plane of poloidal cross-section for small antenna with the height of 11 cm.

If the signs and  $B_0$ , and  $I_p$  are changed simultaneously, then the geometry of spiral of magnetic force line will not change, but the direction of tangential vector of full magnetic field will change to the opposite one. As a result, the projection of the toroidal component of the wave vector  $k_\varphi$  into the perpendicular direction both relative to the vector of full magnetic field and to the  $g$  component gradient of the permittivity tensor of plasma will also change the sign. In heterogenous gyrotropic medium, which is the plasma in a tokamak, such change results in considerable change of dispersion of the wave [14], which, in turn, is manifested as the difference of energy absorption profiles (see fig. 13 and pairs (a) $\leftrightarrow$ (b) and (c) $\leftrightarrow$ (d) in fig. 14). Such effect appears to be very clear in a small spherical tokamak, such as the Globus-M2, where the plasma is very inhomogeneous both in radial, and poloidal directions. (Though we do not give relevant figures, one should note that the change of sign  $n_\varphi$  with the same directions of the magnetic field and current will result in rearrangement of the energy absorption radial profile, and in the inverse rotation direction of the wave cone in the plane of poloidal cross-section.)

The study has also covered the impact of the value of toroidal slowing-down of helicon on its propagation and absorption: determination of an optimum value of  $n_\varphi$  is very important, since it impacts final selection of size and design of the antenna. Profiles of energy absorption depending on the number of toroidal mode  $n_\varphi$  are shown in fig. 15 in one-dimensional, and in fig. 16 in two-dimensional representations, respectively. It is seen, that  $n_\varphi = 20$  and 28 provide a good efficiency of absorption. At  $n_\varphi = 14$  the

efficiency of absorption is reduced a bit, and the interference structure is clearly observed on the 2D profile of absorption, which indicates reflection of wave from the central regions. But it also should be noted that with increase of  $n_\varphi$  the width and height of the barrier of non-transparency region between the vacuum and fast mode cut-off rises, which is not considered herein due to high value of the plasma density at its boundary. Let us recall that only 60% of the supplied power pass through the non-transparency barrier at  $n_\varphi = 28$ . The foregoing allows to conclude that, apparently, the value  $n_\varphi = 20$  is more or less optimum. For excitation of such wave it is required that the antenna structure has the periodicity in the toroidal direction about 20 cm.

Finally, it was checked, how the poloidal size of antenna  $H_{ant}$  impacts propagation and absorption of helicon. Fig. 17 presents comparison of radial profiles of energy absorption for two variants of the antenna: with the reference height  $H_{ant} = 22$  cm and with the height of 11 cm. Fig. 18 shows 2D profiles of full field of wave (fig. 18, a) and absorption (fig. 18, b) for the antenna with the height of 11 cm. For small antenna the efficiency of absorption appeared to be a bit lower, however, in general, there is no big difference versus the reference size.

## Conclusion

Main conclusion that can be made from the analysis of the presented results of full-wave modeling of propagation and absorption of helicons in plasma of the Globus-M2

spherical tokamak is the following. Regardless of a small size of the tokamak, absorption of helicons in main plasma may occur quite efficiently in a wide range of parameters of experiment (as a rule, less than 20% of the HF power is reflected back to the boundary of plasma). At that, the radial profile of energy absorption appears to be wider than in large tokamaks, which somewhat decreases the possibilities of fine control of the current profile. The general recommendation is to use dense hot plasma (central values of density and temperature of at least  $(5-6) \cdot 10^{13} \text{ cm}^{-3}$  and  $(1.5-2) \text{ keV}$  respectively) with optimum magnetic field 8–9 kGs. Wide, flat radial profiles of density and temperature are more favorable than narrow profiles peaked at the discharge axis. Also, it was shown that in a small tokamak, like the Globus-M2, gradient effects play significant role, so one must consider the direction of the wave propagation along the torus relative to directions of the magnetic field and plasma current. Optimum toroidal slowing-down of wave corresponds to excitation of toroidal mode with the number  $n_\phi$  of the order of 20. For this purpose the antenna must excite the traveling (bearing in mind the HF current drive) wave with the length about 20 cm in toroidal direction.

The obtained results are significant in terms of practical application, and will be used in the antenna development and in planning of the experiment the theory and understanding of the specifics of physical processes of propagation and absorption of helicons in plasma of small tokamaks with low aspect ratio. They are also important in terms of application in practice, and will be developed during development of an antenna and planning the experiment with the use of helicons on the Globus-M2 tokamak.

## Funding

The work was funded under state assignment of Ioffe Institute.

## Conflict of interest

The authors declare that they have no conflict of interest.

## References

- [1] V.L. Vdovin. *Fizika plazmy*, **39**, 115 (2013) (in Russian). DOI: 10.7868/S0367292113020030
- [2] R.I. Pinsker. *Phys. Plasmas*, **22**, 090901 (2015). DOI: 10.1063/1.4930135
- [3] C. Lau, E.F. Jaeger, N. Bertelli, L.A. Berry, D.L. Green, M. Murakami, J.M. Park, R.I. Pinsker, R. Prater. *Nucl. Fusion*, **58**, 066004 (2018).
- [4] C. Lau, L.A. Berry, E.F. Jaeger, N. Bertelli. *Plasma Physics Controlled Fusion*, **61** (4), 045008 (2019). DOI: 10.1088/1361-6587/aafd04
- [5] C. Lau, et al. Effects of turbulence in modifying helicon wave CD propagation and efficiency. 28th IAEA Fusion Energy Conference (FEC 2020), 10–15 May 2021.
- [6] C. Gormezano, A.C.C. Sips, T.C. Luce, S. Ide, A. Becoulet, X. Litaudon, A. Isayama, J. Hobirk, M.R. Wade, T. Oikawa, R. Prater, A. Zvonkov, B. Lloyd, T. Suzuki, E. Barbato, P. Bonoli, C.K. Phillips, V. Vdovin, E. Joffrin, T. Casper, J. Ferron, D. Mazon, D. Moreau, R. Bundy, C. Kessel, A. Fukuyama, N. Hayashi, F. Imbeaux, M. Murakami, A.R. Polevoi, H.E. St John. *Nucl. Fusion*, **47** (6), S285 (2007). DOI: 10.1088/0029-5515/47/6/S06
- [7] R.I. Pinsker. *Review of tokamak experiments on direct electron heating and current drive with fast waves. Proceedings of the 10th Topical Conference on Radio Frequency Power in Plasmas*, Boston, MA, 1993 (American Institute of Physics, NY., 1994), p. 179.
- [8] M. Ono. *Phys. Plasmas*, **2** (11), 4075 (1995). DOI: 10.1063/1.871030
- [9] V.E. Golant. *ZhTF*, **41**, 2492 (1971) (in Russian).
- [10] V.B. Minaev, V.K. Gusev, N.V. Sakharov, V.I. Varfolomeev, N.N. Bakharev, V.A. Belyakov, E.N. Bondarchuk, P.N. Brunkov, F.V. Chernyshev, V.I. Davydenko, V.V. Dyachenko, A.A. Kavin, S.A. Khitrov, N.A. Khromov, E.O. Kiselev, A.N. Konovalov, V.A. Kornev, G.S. Kurskiy, A.N. Labusov, A.D. Melnik, A.B. Mineev, M.I. Mironov, I.V. Miroschnikov, M.I. Patrov, Yu.V. Petrov, V.A. Rozhansky, A.N. Saveliev, I.Yu. Senichenkov, P.B. Shchegolev, O.N. Shcherbinin, I.V. Shikhovtsev, A.D. Sladkomedova, V.V. Solokha, V.N. Tanchuk, A.Yu. Telnova, V.A. Tokarev, S.Yu. Tolstyakov, E.G. Zhilin. *Nucl. Fusion*, **57** (6), 066047 (2017). DOI: 10.1088/1741-4326/aa69e0
- [11] N.N. Bakharev, I.M. Balachenkov, V.I. Varfolomeev. *Fizika plazmy*, **46** (7), 579 (2020) (in Russian). DOI: 10.31857/S036729212007001X
- [12] E.Z. Gusakov, V.V. Dyachenko, M.A. Irzak, S.A. Khitrov, A.N. Saveliev, O.N. Shcherbinin. *Plasma Phys. Controlled Fusion*, **52** (7), 075018 (2010). DOI: 10.1088/0741-3335/52/7/075018
- [13] M. Brambilla. *Plasma Phys. Controlled Fusion*, **41** (1), 1 (1999). DOI: 10.1088/0741-3335/41/1/002
- [14] E.Z. Gusakov, M.A. Irzak, A.D. Piliya. *J. Experiment. Theor. Phys. Lett.*, **65**, 25 (1997).